Determining the impact of gold nanoparticles on amyloid aggregation with 2D IR spectroscopy

Special Collection: Celebrating 25 Years of Two-dimensional Infrared (2D IR) Spectroscopy

Kayla A. Hess ; Nathan J. Spear ; Sophia A. Vogelsang ; Janet E. Macdonald ;
Lauren E. Buchanan

Check for updates

View Online   Export Citation

28 March 2024 18:01:23

Determining the impact of gold nanoparticles on amyloid aggregation with 2D IR spectroscopy

Kayla A. Hess, [iD] Nathan J. Spear, [iD] Sophia A. Vogelsang, [iD] Janet E. Macdonald, [iD] and Lauren E. Buchanan[a) [iD]

AFFILIATIONS

Department of Chemistry, Vanderbilt University, 1234 Stevenson Center Lane, Nashville, Tennessee 37235, USA

Note: This paper is part of the JCP Special Topic on Celebrating 25 Years of Two-Dimensional Infrared (2D IR) Spectroscopy.
[a)]Author to whom correspondence should be addressed: lauren.e.buchanan@vanderbilt.edu

ABSTRACT

As nanomaterials become more prevalent in both industry and medicine, it is crucial to fully understand their health risks. One area of concern is the interaction of nanoparticles with proteins, including their ability to modulate the uncontrolled aggregation of amyloid proteins associated with diseases, such as Alzheimer's disease and type II diabetes, and potentially extend the lifetime of cytotoxic soluble oligomers. This work demonstrates that two-dimensional infrared spectroscopy and $^{13}C^{18}O$ isotope labeling can be used to follow the aggregation of human islet amyloid polypeptide (hIAPP) in the presence of gold nanoparticles (AuNPs) with single-residue structural resolution. 60 nm AuNPs were found to inhibit hIAPP, tripling the aggregation time. Furthermore, calculating the actual transition dipole strength of the backbone amide I' mode reveals that hIAPP forms a more ordered aggregate structure in the presence of AuNPs. Ultimately, such studies can provide insight into how mechanisms of amyloid aggregation are altered in the presence of nanoparticles, furthering our understanding of protein–nanoparticle interactions.

Published under an exclusive license by AIP Publishing. https://doi.org/10.1063/5.0136376

I. INTRODUCTION

Due to their uniquely tunable chemical and optical properties,[1] nanomaterials are found in applications as diverse as cosmetics,[2] food science,[3] and nanomedicine. The scale of nanoparticles (NPs) allows them to cross biological barriers, including cellular membranes and the blood–brain barrier.[4–6] While this property enables many biomedical applications of NPs, including drug delivery,[7–9] diagnostics,[10–12] and imaging,[13–15] it can also make NPs difficult to control within the body. Off-target NPs often accumulate in the liver or spleen,[16,17] and metal NPs can have a cytotoxic impact on liver cells.[18] Various NPs, including metal NPs, pose additional cytotoxic risks to the reproductive system[19] and the brain.[20,21] One possible cause of NP toxicity is the accumulation of proteins on the NP surface, leading to local increases in protein concentration and structural changes.[22–27] Structural changes can impact protein function by several means, such as disrupting the cell surface receptors that bind NP–protein complexes[22] or increasing thermal stability to prevent fibrillation at higher temperatures,[26] but these effects depend on NP characteristics, such as surface chemistry, size, and relative concentration, and the protein itself. As the impact of a particular combination of factors is challenging to predict, it is vital to develop

methods capable of probing the structural effects of NP–protein interactions to prevent adverse outcomes of NP exposure.

Of particular concern is the interaction of NPs with amyloidogenic proteins associated with Alzheimer's disease, Parkinson's disease, type II diabetes, and other diseases that are characterized by the misfolding and aggregation of proteins into extended β-sheet-rich fibrils.[28] While studies have demonstrated that amyloid aggregation can be either accelerated or inhibited by the presence of NPs, depending on their specific properties and the protein of interest,[29,30] little is known about the mechanism of interaction. One hypothesis is that NPs provide a seed surface that accelerates the rate of fibril formation, although factors, such as NP size and curvature, determine that acceleration.[31] Yet, adsorption of proteins onto the NP surface depletes their concentration in solution, which may inhibit aggregation. It is unknown, however, which species are trapped on the NP surface. In the case of monomer binding, the monomer–oligomer equilibrium is disrupted, forcing oligomeric species in solution to dissociate back into monomers.[32] However, for oligomer binding, the opposite would be true and equilibrium would favor the formation of more oligomers. Additionally, the bound oligomers may persist longer than usual due to being trapped

on the NP surface.[32] Critically, soluble prefibrillar oligomers have been shown to be the most cytotoxic species in these diseases;[33–36] thus, NPs that prolong the lifetime of such oligomers could lead to increased toxicity.

Gold nanoparticles (AuNPs) are commonly studied in nanomedicine for use in biosensing,[37–40] drug delivery,[41–44] and imaging.[44–46] Additionally, they serve as a convenient model system for biophysical studies due to their lack of spectroscopic signatures that may interfere with protein signals. The effects of AuNPs on amyloid aggregation have been demonstrated[47] to vary between acceleration and inhibition depending on both size and surface chemistry, as well as between different amyloidogenic proteins. Several studies have examined the interactions of AuNPs with human islet amyloid polypeptide (hIAPP) [Fig. 1(a)], a 37-residue peptide associated with type II diabetes.[31,48–51] Two of these examined the interactions of 5 or 20 nm citrate-capped AuNPs with a seven-residue fragment (NNFGAIL) from the "amyloid core" of hIAPP using Thioflavin T (ThT) fluorescence assays and found that aggregation was accelerated in the presence of AuNPs.[31,49] Another study used circular dichroism spectroscopy to reveal that full-length hIAPP adopted ordered secondary structures (both α-helices and β-sheets) more quickly when aggregated in the presence of 5–10 nm citrate-capped AuNPs.[48] While the formation of fibrils was confirmed using transmission electron microscopy (TEM), α-helical configurations appeared to persist when AuNPs were present. Yet another study observed inhibition of hIAPP aggregation by both negatively charged, carboxyl-functionalized and positively charged, amine-functionalized 30 nm AuNPs via ThT assays.[50] However, none of these studies were able to determine the mechanisms by which AuNPs alter hIAPP aggregation, leaving questions about whether their interaction may be beneficial or harmful.

Fully understanding how NPs affect amyloid aggregation pathways requires experimental techniques capable of simultaneous structural and temporal resolution sufficient to identify and track transient oligomer species. ThT assays, commonly used to monitor amyloid kinetics, provide limited structural information beyond identifying the presence of amyloid β-sheets.[32,52] Techniques with high structural resolution, such as x-ray crystallography,[53,54] solid-state nuclear magnetic resonance (ssNMR) spectroscopy,[55,56] and cryo-electron microscopy,[57,58] have limited temporal resolution and are more readily applied to stable or isolated aggregates. In the case of NMR, NPs further complicate spectral interpretation due peak broadening caused by slower tumbling of the NP–protein complexes.[59] In contrast, two-dimensional infrared (2D IR) spectroscopy coupled with site-specific isotope labeling has the requisite structural and temporal resolution to probe the mechanism of amyloid aggregation and identify both transient intermediates and structural polymorphs.[60–64] Moreover, 2D IR of NP-bound peptides has been demonstrated as a means to determine the β-sheet-like structure of a tripeptide on the surface of silver NPs when compared to the peptide in free solution.[65,66] Small amide and carboxyl capping ligands have also been characterized on the surface of gold NPs using 2D IR, revealing that the dynamics of capping ligands change at the NP surface.[67] This work further advances the field by demonstrating that 2D IR spectroscopy can be used to continuously monitor the aggregation of a full-length amyloid peptide, hIAPP, in the presence of AuNPs and determine how the final structures may be altered.

II. METHODS

A full description of methods is given in the supplementary material. Briefly, hIAPP was synthesized using standard Fmoc solid-phase peptide synthesis (SPPS) and purified via high performance liquid chromatography.[68] Fmoc-protected $^{13}C^{18}O$-labeled valine was prepared for incorporation via SPPS according to established
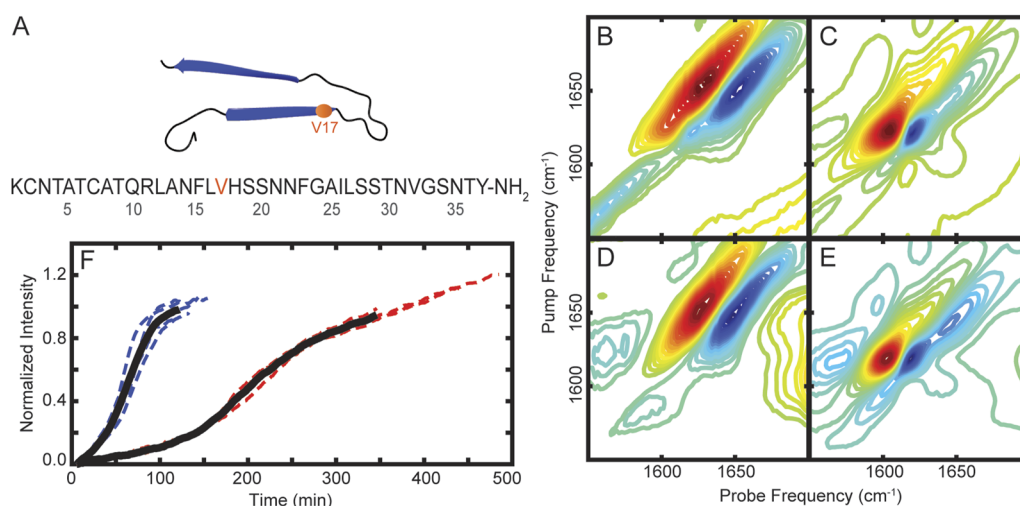
FIG. 1. (a) Sequence and structural model of hIAPP fibrils derived from ssNMR,[55] with residue V17 highlighted in orange. 2D IR spectra of UL hIAPP without AuNPs after (b) 10 min and (c) 2 h of aggregation. 2D IR spectra of UL hIAPP with 60 nm AuNPs after (d) 10 min and (e) 6 h of aggregation. (f) Aggregation kinetics of hIAPP fibrils without (blue) and with (red) AuNPs, monitored at the 1619 cm^{-1} β-sheet peak and normalized such that the intensity at $t_{0.5}$ equals 0.5. The average kinetic trace for five replicates at each condition are plotted in black.

methods, starting from commercial ^{13}C-valine.[69] AuNPs were synthesized in water using a modified version of established literature methods,[70] yielding 60 ± 10 nm AuNPs according to TEM (Figs. S1 and S2) and UV–vis characterization.[71]

hIAPP samples were dissolved in deuterated hexafluoroisopropanol (dHFIP) to fully disaggregate any fibrils. To initiate aggregation, dHFIP was removed by lyophilization and the dry peptide was reconstituted in 20 mM deuterated Tris buffer (pH ~7.6) at a final concentration of 1 mM. For nanoparticle experiments, AuNP stock solution was washed three times with D_2O and resuspended in 20 mM deuterated Tris buffer to obtain a final concentration of 2.08 × 10^{12} NPs/ml. Lyophilized hIAPP was then dissolved in the AuNP solution to achieve a final peptide concentration of 1 mM.

The 2D IR system has been described previously, as have detailed methods for 2D IR data collection and processing.[69,72] For aggregation runs, spectra were continuously collected for ~2 h without AuNPs or 6–8 h with AuNPs. Detailed methods for calculation of transition dipole strength (TDS) spectra have previously been described.[73,74]

III. RESULTS AND DISCUSSION

We first used 2D IR spectroscopy to monitor the aggregation of unlabeled (UL) hIAPP without AuNPs. Spectra of the amide I' mode of hIAPP are shown in Fig. 1. In infrared spectra, the frequency of the amide I' mode, which largely comprises backbone C=O stretching, depends strongly on the secondary structure: disordered peptides absorb near 1645–1650 cm^{-1} while the extended β-sheets present in amyloid fibrils absorb near 1620–1630 cm^{-1}.[60,62,63] After only 10 min of aggregation [Fig. 1(b)], UL hIAPP exhibits a pair of broad peaks at 1650 cm^{-1} that is characteristic of disordered peptides and a weak peak pair at 1619 cm^{-1} that indicates initial formation of β-sheet structures. After 2 h of aggregation [Fig. 1(c)], UL hIAPP displays a strong peak pair at 1619 cm^{-1}, characteristic of extended β-sheets present in amyloid fibrils, while a weak shoulder at ~1650 cm^{-1} indicates that some disordered structures persist. This fiber spectrum is consistent with known structural models based on 2D IR and ssNMR spectra.[55,60–63] Within the final fibrils, each monomer forms two β-sheets spanning residues 8–17 and 25–37 connected by a partially disordered loop structure [Fig. 1(a)].

As an initial test to determine how AuNPs alter hIAPP structure, UL hIAPP was aggregated in the presence of 60 nm citrate-capped AuNPs. At the 1 mM peptide concentration used, there was an excess of hIAPP to AuNPs on the order of 28 000:1, where monolayer surface coverage corresponds to ~900 peptides per AuNP. 2D IR spectra of the AuNPs confirmed that they do not absorb in the amide I' region (Fig. S3) and thus do not interfere with interpretation of peptide spectral features. After 10 min of aggregation [Fig. 1(d)], UL hIAPP mixed with AuNPs displays a pair of broad peaks at 1648 cm^{-1} that correspond to disordered structures. In contrast to the spectrum of hIAPP without AuNPs [Fig. 1(b)], however, there are no clear peaks around 1620 cm^{-1}, suggesting that early β-sheet structures have not yet begun to form. After 2 h of aggregation (Fig. S4), UL hIAPP with AuNPs remain largely disordered. After 6 h of aggregation [Fig. 1(e)], UL hIAPP with AuNPs does display a strong peak pair at 1619 cm^{-1} characteristic of amyloid fibrils, but the high-frequency shoulder representing disordered structures remains more distinct compared to spectra obtained when AuNPs were not

present [Fig. 1(c)]. The formation of amyloid fibrils in the presence of AuNPs was confirmed via TEM (Fig. S1C). While amyloid fibrils formed with and without AuNPs present produced similar 2D IR spectra, the time scales between the two conditions clearly differed, requiring continuous collection of 2D IR spectra throughout the aggregation process to measure aggregation kinetics and thus better understand how AuNPs impact hIAPP aggregation.

The intensity of the β-sheet peak at 1619 cm^{-1} can be monitored as a function of time to track amyloid aggregation [Fig. 1(f)], equivalent to traditional ThT fluorescence measurements.[60,62,63] The data were fit to a sigmoidal function [Eq. (1)] where y_0 is initial baseline intensity, A is the amplitude of the increase, k is the apparent growth rate, and $t_{0.5}$ is the midpoint of the growth curve,[75–77]

$$y = y_0 + \frac{A}{1 + e^{-k(t - t_{0.5})}}. \qquad (1)$$

Each run was terminated when the intensity of the β-sheet peak plateaued, suggesting that the solution had achieved equilibrium. With AuNPs present, however, the solution never appeared to reach a stable equilibrium after the growth phase, as indicated by a continued gradual increase in the intensity of the β-sheet peak for up to 8 h [Fig. 1(f), red]. To ensure consistency in fitting between replicates, all AuNP kinetic traces were truncated after 350 min to match the shortest aggregation run. Without AuNPs present, the average $t_{0.5}$ over 5 replicates was 63 ± 5 min [Fig. 1(f), blue]. In the presence of 60 nm AuNPs, the average $t_{0.5}$ increased to 203 ± 10 min [Fig. 1(f), red]. Therefore, the presence of the 60 nm AuNPs, even with a 28 000:1 excess of peptide:NP slowed hIAPP aggregation by nearly a factor of three. When AuNPs were present, the intensity of the β-sheet peak continued to steadily increase after the rapid growth phase was complete and did not reach a true equilibrium even after 8 h. This deviation from standard sigmoidal growth could indicate that fibrils simply elongate more slowly following the initial growth phase or that the mechanism of aggregation may be more dramatically altered, in that the incorporation of some residues into the fibrillar β-sheets could be delayed. TEM images of the AuNPs showed that the protein capping layer consistently remained around 7 nm over the course of 24 h (Fig. S2), indicating that the continued slow increase in β-sheet intensity does not arise from the gradual desorption of proteins from the surface and their subsequent incorporation into the fibrils. However, these hypothetical mechanisms cannot be differentiated using UL hIAPP as the amide I' modes of each residue are identical and no single residue can be distinguished from the rest of the peptide. To achieve residue-level structural resolution, we can incorporate site-specific isotope labels.

When individual residues are labeled with [13]C[18]O at the backbone carbonyl, the increased mass leads to a ~60 cm^{-1} shift in amide I' frequency, spectrally isolating the labeled residue from the rest of the peptide.[69,78–80] This approach has been demonstrated to increase the structural resolution of 2D IR to the level of single residues in mechanistic studies of amyloid aggregation,[60,62,63] investigations into membrane proteins[81,82] and α-helices,[83,84] and the identification of structural differences in polymorphic peptide aggregates.[61,72] Additionally, isotope-labeling has been used to determine the static structure of a self-assembled tripeptide monolayer on the surface of silver NPs.[66] This work demonstrates that [13]C[18]O isotope-labeling

28 March 2024 18:01:23

with 2D IR spectroscopy is capable of tracking residue-level structural changes during protein aggregation in the presence of NPs. A $^{13}C^{18}O$ isotope label was inserted in hIAPP at valine-17 (V17). Based on existing structural models,[55,60–63] V17 falls within the N-terminal β-sheet of hIAPP fibrils [Fig. 1(a)]. Thus, as hIAPP aggregates, the V17 residue shifts from a disordered structure to β-sheet structure and the labeled amide I' mode redshifts correspondingly in 2D IR spectra.[60–62] After 10 min of aggregation without AuNPs [Fig. 2(a)], the $^{13}C^{18}O$ label appears as a weak peak pair at 1582 cm^{-1}, which, along with the presence of weak β-sheet peaks at 1619 cm^{-1} for the UL amide I' mode, indicates initial formation of β-sheet structures at V17. The $^{13}C^{18}O$ mode corresponding to V17 in a disordered structure appears as a broad peak pair around 1595 cm^{-1} but is significantly weaker than the other spectral features and not well-resolved. After 2 h of aggregation [Fig. 2(b)], the labeled amide I' mode at 1582 cm^{-1} is stronger and well-defined corresponding to full incorporation of V17 into the fibril β-sheets. The UL amide I' mode appears as a strong peak pair at 1619 cm^{-1}, as expected from spectra of UL hIAPP [Fig. 1(c)]. Similar behavior is observed in the presence of AuNPs [Figs. 2(c) and 2(d)]. Critically, the isotope-labeled mode appears at the same frequency within the final fibers both with and without AuNPs, indicating that V17 adopts a similar structure within the fibril β-sheets even when aggregation is inhibited.

The rate of V17 incorporation into the fibril β-sheets can be tracked using the intensity of the $^{13}C^{18}O$ mode at 1582 cm^{-1}. Kinetic traces of the V17 label were found to follow the same general trends displayed by the unlabeled amide I' β-sheet peak at 1619 cm^{-1} [Fig. 2(e)], with AuNPs slowing the rate that V17 is incorporated into the fibril β-sheets by a factor of three. Furthermore, in the presence of AuNPs, the intensity of the V17 peak continues to slowly increase after the rapid growth phase, matching with the trend observed for overall fibril formation. Previous mechanistic studies of hIAPP aggregation found that the V17 residue was among the first residues to be incorporated into the β-sheet when compared to other labeled residues.[62] The V17 continues to track with overall fibril formation, suggesting that AuNPs do not significantly alter early stages of aggregation. The continued increase in intensity is due either to a more gradual elongation of the fibrils once the core structure has been formed or residues closer to the termini, known to adopt β-sheet structures slower than the central residues, may be delayed in adopting their final structures.

The similarities between the 2D IR spectra in Figs. 1 and 2 indicate that, regardless of whether aggregation is inhibited by AuNPs or not, hIAPP forms fibrils with similar overall β-sheet structures and similar structures at the V17 residue, specifically. However, several studies have shown that TDS are more sensitive than vibrational frequencies to differences in protein secondary structure.[73,74,85,86] Both frequency shifts and changes in TDS arise from differences in vibrational couplings between the amide I' modes within ordered protein structures.[73] These couplings strongly depend on the residue dihedral angles and the relative distance and orientations of the amide I' groups. In extended structures, such as amyloid fibrils, however, frequency shifts reach an asymptotic limit and the observed frequency is primarily determined by the average magnitude of the vibrational couplings, i.e., the average structure. In contrast, TDS is sensitive to small variations in coupling around these average values;[85] larger variations lead to decreased delocalization of the vibrational modes
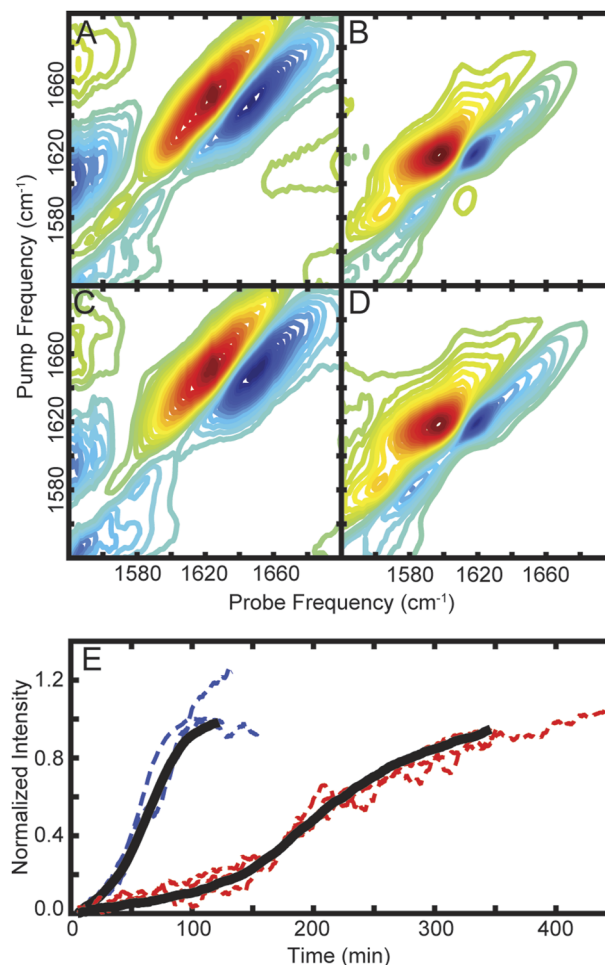

FIG. 2. 2D IR spectra of V17 hIAPP without AuNPs after (a) 10 min and (b) 2 h of aggregation. 2D IR spectra of V17 hIAPP with 60 nm AuNPs after (c) 10 min and (d) 6 h of aggregation. (e) Aggregation kinetics of V17 incorporation into fibril β-sheets without (blue) and with (red) AuNPs, monitored at 1582 cm^{-1} and normalized such that the intensity at $t_{0.5}$ equals 0.5. The average kinetic trace of the UL β-sheet peak at 1620 cm^{-1} is plotted in black for comparison at each condition.

and thus weaker TDS. Therefore, increased ordering of an amyloid β-sheet can lead to higher TDS values, even when overall structure, and thus the vibrational frequency, remains unchanged. Previously, TDS calculations have been used to differentiate between disordered and α-helical structures, despite their overlap in vibrational frequency, and reveal the presence of structural polymorphs within β-sheet aggregates that were invisible to other techniques.[74]

First, to determine if AuNPs enhance amide I' signal, and thus the calculated TDS, the TDS of N-methylacetamide (NMA), a well-established model of uncoupled amide bonds with a documented TDS of 0.12 D^2,[73,86] was calculated with and without AuNPs. Across three replicates, the average TDS was found to be 0.12 D^2 regardless of whether AuNPs were present (Fig. S5), suggesting that AuNPs do not affect TDS values. The lack of enhancement is further supported
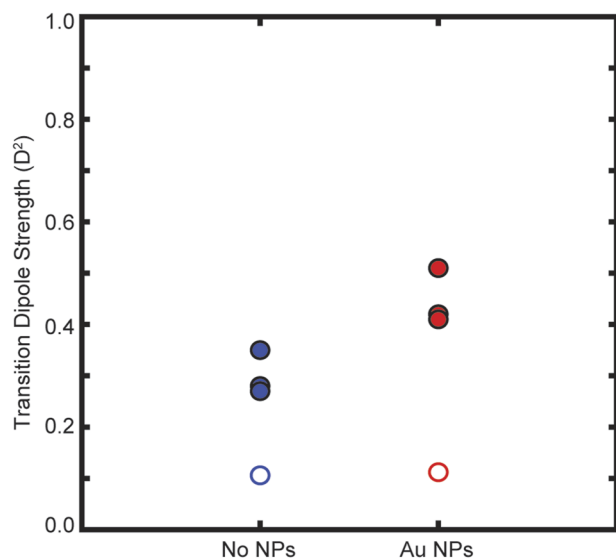
28 March 2024 18:01:23

FIG. 3. Comparison of amide I' TDS values for hIAPP without (blue) and with (red) AuNPs present. TDS of lag-phase hIAPP (empty circles) was calculated at 1648 cm^{-1} after 10 min of aggregation, while TDS of aggregated hIAPP fibrils (filled circles) was calculated at 195 min without AuNPs and 455 min with AuNPs.

by comparing TDS values for hIAPP with and without AuNPs during the lag phase, during which time the peptide is primarily found in a disordered, monomeric state [Figs. 1(b) and 1(d)]. For both conditions, the TDS was found to be ~0.11 D^2 (Fig. 3, empty circles), which is comparable to the fully uncoupled value observed for NMA. While the disordered protein may not absorb onto the AuNP surface in exactly the same manner as at later times when fibrils are present, these results again indicate that AuNPs do not significantly enhance 2D IR signals or change the calculated TDS values.

Having confirmed that TDS is not affected by the presence of AuNPs, TDS spectra of the final hIAPP aggregates formed with and without AuNPs were calculated. As all TDS spectra of aggregated hIAPP exhibit a single maximum within the β-sheet spectral region (Fig. S6), we can simply compare the maximum TDS values (Fig. 3, filled circles). Over three replicates, hIAPP fibrils formed without AuNPs exhibited an average TDS of 0.30 ± 0.04 D^2 when measured after 195 min of aggregation. In comparison, fibrils formed with AuNPs present displayed an average TDS of 0.45 ± 0.05 D^2 when measured after 455 min of aggregation. The variation in TDS values observed for each condition is comparable to or smaller than variations reported for other amyloid proteins.[73,85] A higher TDS value indicates greater delocalization of the amide I' mode and, when considered in combination with the identical vibrational frequencies between fibrils formed with and without AuNPs, suggest that the β-sheets within hIAPP fibrils are similarly structured, but more highly ordered, when formed in the presence of AuNPs. Slower aggregation in the presence of AuNPs may allow the individual peptide monomers more time to adopt an optimal configuration as they come into alignment within the fibril β-sheets, resulting in a more uniform overall structure. Furthermore, when AuNPs were present, the fibril TDS continued to increase after the sigmoidal growth phase (Fig. S7), from 0.34 D^2 to 0.45 D^2 over the course of 100 min. In

contrast, TDS of fibrils grown without AuNPs remained constant after the growth phase (Fig. S8). Given that the length of the fibrils is already far longer than the delocalization length of 3–4 residues, this increase does not indicate that the fibril is lengthening but rather that the structure is continuing to become more rigid.

IV. CONCLUSIONS

As nanomaterials become increasingly ubiquitous in commercial, industrial, and medical applications, it is vital to understand how they interact with and affect the molecules that underlie all biological functions. In particular, proteins are known undergo structural changes when adsorbed onto NP surfaces,[22–27] which may affect their native function or create new toxic effects. Here, we demonstrate that 2D IR spectroscopy can be used to continuously monitor residue-level structural changes during the aggregation of a full-length amyloid peptide, hIAPP, in the presence of AuNPs. Using TDS calculations and isotope-labeling, we found that 60 nm AuNPs do not significantly alter the structure of hIAPP fibrils, but that the final fibrils do appear to be more ordered. This may arise simply from the slower aggregation process allowing more time for individual peptides to adopt an optimal configuration or may indicate that AuNPs subtly alter the aggregation pathway. Previous research has identified at least two structural polymorphs of hIAPP that result from diverging aggregation pathways; in that study, the amide I' mode of V17 was insensitive to the different fibril structures, but those of alanine-25 were highly dependent on changes in aggregation conditions.[61] As both the structure and kinetics of V17 incorporation into the fibril β-sheets appears unchanged in the presence of AuNPs, differentiating between the possible mechanisms of inhibition remains the subject of ongoing investigations with a wider range of isotope-labeled residues, including alanine-25. Understanding changes to amyloid aggregation pathways, including the structures of species that are kinetically trapped by binding to the NP surface and different polymorphs that may arise, is critical to understanding NP toxicity and the development of therapeutics.

SUPPLEMENTARY MATERIAL

See the supplementary material for detailed materials and methods, TEM spectra of AuNPs and hIAPP fibrils, additional 2D IR spectra, and sample TDS spectra.

AUTHOR DECLARATIONS

Conflict of Interest

The authors have no conflicts to disclose.

28 March 2024 18:01:23

Author Contributions

DATA AVAILABILITY

The data that support the findings of this study are available from the corresponding author upon reasonable request.

REFERENCES

[1] J. Jeevanandam, A. Barhoum, Y. S. Chan, A. Dufresne, and M. K. Danquah, Beilstein J. Nanotechnol. **9**, 1050 (2018).

[2] Z. A. A. Aziz, H. Mohd-Nasir, A. Ahmad, S. H. M. Setapar, W. L. Peng, S. C. Chuo, A. Khatoon, K. Umar, A. A. Yaqoob, and M. N. Mohamad Ibrahim, Front. Chem. **7**, 739 (2019).

[3] T. Singh, S. Shukla, P. Kumar, V. Wahla, V. K. Bajpai, and I. A. Rather, "Application of nanotechnology in food science: Perception and overview," Front. Microbiol. **8**, 1501 (2017).

[4] Z. Zhao, A. Ukidve, V. Krishnan, and S. Mitragotri, Adv. Drug Delivery Rev. **143**, 3 (2019).

[5] L. Wang and C. Chen, Toxicol. Appl. Pharmacol. **299**, 30 (2016).

[6] J. Xie, Z. Shen, Y. Anraku, K. Kataoka, and X. Chen, Biomaterials **224**, 119491 (2019).

[7] D. Bobo, K. J. Robinson, J. Islam, K. J. Thurecht, and S. R. Corrie, Pharm. Res. **33**, 2373 (2016).

[8] M. J. Mitchell, M. M. Billingsley, R. M. Haley, M. E. Wechsler, N. A. Peppas, and R. Langer, Nat. Rev. Drug Discovery **20**, 101 (2021).

[9] J. K. Patra, G. Das, L. F. Fraceto, E. V. R. Campos, M. del P. Rodriguez-Torres, L. S. Acosta-Torres, L. A. Diaz-Torres, R. Grillo, M. K. Swamy, S. Sharma, S. Habtemariam, and H. S. Shin, J. Nanobiotechnol. **16**, 71 (2018).

[10] P. D. Howes, S. Rana, and M. M. Stevens, Chem. Soc. Rev. **43**, 3835 (2014).

[11] P. D. Howes, R. Chandrawati, and M. M. Stevens, Science **346**, 1247390 (2014).

[12] N. L. Rosi and C. A. Mirkin, Chem. Rev. **105**, 1547 (2005).

[13] E. Phillips, O. Penate-Medina, P. B. Zanzonico, R. D. Carvajal, P. Mohan, Y. Ye, J. Humm, M. Gönen, H. Kalaigian, H. Schöder, H. W. Strauss, S. M. Larson, U. Wiesner, and M. S. Bradbury, Sci. Transl. Med. **6**, 260ra149 (2014).

[14] Y. Yang, L. Wang, B. Wan, Y. Gu, and X. Li, Front. Bioeng. Biotechnol. **7**, 320 (2019).

[15] M. Bruchez, M. Moronne, P. Gin, S. Weiss, and A. P. Alivisatos, Science **281**, 2013 (1998).

[16] E. Blanco, H. Shen, and M. Ferrari, Nat. Biotechnol. **33**, 941 (2015).

[17] S. Parveen, R. Misra, and S. K. Sahoo, Nanomed. Nanotechnol., Biol. Med. **8**, 147 (2012).

[18] S. M. Hussain, K. L. Hess, J. M. Gearhart, K. T. Geiss, and J. J. Schlager, Toxicol. In Vitro **19**, 975 (2005).

[19] R. Wang, B. Song, J. Wu, Y. Zhang, A. Chen, and L. Shao, Int. J. Nanomed. **13**, 8487 (2018).

[20] B. A. Maher, I. A. M. Ahmed, V. Karloukovski, D. A. MacLaren, P. G. Foulds, D. Allsop, D. M. A. Mann, R. Torres-Jardón, and L. Calderon-Garciduenas, Proc. Natl. Acad. Sci. U. S. A. **113**, 10797 (2016).

[21] Q. Gu, E. Cuevas, S. F. Ali, M. G. Paule, V. Krauthamer, Y. Jones, and Y. Zhang, Int. J. Toxicol. **38**, 385 (2019).

[22] C. C. Fleischer and C. K. Payne, J. Phys. Chem. B **118**, 14017 (2014).

[23] M. Falahati, F. Attar, M. Sharifi, T. Haertlé, J.-F. Berret, R. H. Khan, and A. A. Saboury, Biochim. Biophys. Acta, Gen. Subj. **1863**, 971 (2019).

[24] N. Brandes, P. B. Welzel, C. Werner, and L. W. Kroh, J. Colloid Interface Sci. **299**, 56 (2006).

[25] M. Vitali, V. Rigamonti, A. Natalello, B. Colzani, S. Avvakumova, S. Brocca, C. Santambrogio, J. Narkiewicz, G. Legname, M. Colombo, D. Prosperi, and R. Grandori, Biochim. Biophys. Acta, Gen. Subj. **1862**, 1556 (2018).

[26] S. Goy-López, J. Juárez, M. Alatorre-Meda, E. Casals, V. F. Puntes, P. Taboada, and V. Mosquera, Langmuir **28**, 9113 (2012).

[27] Y. Zhang, J. L. Y. Wu, J. Lazarovits, and W. C. W. Chan, J. Am. Chem. Soc. **142**, 8827 (2020).

[28] F. Chiti and C. M. Dobson, Annu. Rev. Biochem. **86**, 27 (2017).

[29] A. Gladytz, B. Abel, and H. J. Risselada, Angew. Chem. **55**, 11242 (2016).

[30] B. Wang, E. H. Pilkington, Y. Sun, T. P. Davis, P. C. Ke, and F. Ding, Environ. Sci.: Nano **4**, 1772 (2017).

[31] T. John, J. Adler, C. Elsner, J. Petzold, M. Krueger, L. L. Martin, D. Huster, H. J. Risselada, and B. Abel, J. Colloid Interface Sci. **622**, 804 (2022).

[32] C. Cabaleiro-Lago, F. Quinlan-Pluck, I. Lynch, S. Lindman, A. M. Minogue, E. Thulin, D. M. Walsh, K. A. Dawson, and S. Linse, J. Am. Chem. Soc. **130**, 15437 (2008).

[33] G. G. Glenner, E. David Eanes, and C. A. Wiley, Biochem. Biophys. Res. Commun. **155**, 608 (1988).

[34] P. Westermark, U. Engström, K. H. Johnson, G. T. Westermark, and C. Betsholtz, Proc. Natl. Acad. Sci. U. S. A. **87**, 5036 (1990).

[35] R. Kayed, E. Head, J. L. Thompson, T. M. McIntire, S. C. Milton, C. W. Cotman, and C. G. Glabe, Science **300**, 486 (2003).

[36] B. Konarkowska, J. F. Aitken, J. Kistler, S. Zhang, and G. J. S. Cooper, FEBS J. **273**, 3614 (2006).

[37] J. E. Kim, J. H. Choi, M. Colas, D. H. Kim, and H. Lee, Biosens. Bioelectron. **80**, 543 (2016).

[38] E. Karakuş, E. Erdemir, N. Demirbilek, and L. Liv, Anal. Chim. Acta **1182**, 338939 (2021).

[39] Q. Wang, F. Min, and J. Zhu, Mater. Lett. **91**, 9 (2013).

[40] R. Jalili, S. Chenaghlou, A. Khataee, B. Khalilzadeh, and M.-R. Rashidi, Molecules **27**, 431 (2022).

[41] P. Manivasagan, S. Bharathiraja, N. Q. Bui, B. Jang, Y.-O. Oh, I. G. Lim, and J. Oh, Int. J. Biol. Macromol. **91**, 578 (2016).

[42] J. Song, J. Zhou, and H. Duan, J. Am. Chem. Soc. **134**, 13458 (2012).

[43] Z. Han, M. Gao, Z. Wang, L. Peng, Y. Zhao, and L. Sun, J. Drug Delivery Sci. Technol. **75**, 103610 (2022).

[44] A. Topete, M. Alatorre-Meda, P. Iglesias, E. M. Villar-Alvarez, S. Barbosa, J. A. Costoya, P. Taboada, and V. Mosquera, ACS Nano **8**, 2725 (2014).

[45] L.-Y. Chen, C.-W. Wang, Z. Yuan, and H.-T. Chang, Anal. Chem. **87**, 216 (2015).

[46] Y. Zhang, J. Qian, D. Wang, Y. Wang, and S. He, Angew. Chem., Int. Ed. **52**, 1148 (2013).

[47] T. John, A. Gladytz, C. Kubeil, L. L. Martin, H. J. Risselada, and B. Abel, Nanoscale **10**, 20894 (2018).

[48] S.-T. Wang, Y. Lin, N. Todorova, Y. Xu, M. Mazo, S. Rana, V. Leonardo, N. Amdursky, C. D. Spicer, B. D. Alexander, A. A. Edwards, S. J. Matthews, I. Yarovsky, and M. M. Stevens, Chem. Mater. **29**, 1550 (2017).

[49] A. Gladytz, M. Wagner, T. Häupl, C. Elsner, and B. Abel, Part. Part. Syst. Charact. **32**, 573 (2015).

[50] Y. Peretz, R. Malishev, S. Kolusheva, and R. Jelinek, Biochim. Biophys. Acta, Biomembr. **1860**, 1810 (2018).

[51] I. Javed, J. He, A. Kakinen, A. Faridi, W. Yang, T. P. Davis, P. C. Ke, and P. Chen, ACS Appl. Mater. Interfaces **11**, 10462 (2019).

[52] E. Lipiec, *Vibrational Spectroscopy in Protein Research* (Academic Press, 2020), pp. 249–268.

[53] R. Nelson, M. R. Sawaya, M. Balbirnie, A. Ø. Madsen, C. Riekel, R. Grothe, and D. Eisenberg, Nature **435**, 773 (2005).

[54] M. R. Sawaya, S. Sambashivan, R. Nelson, M. I. Ivanova, S. A. Sievers, M. I. Apostol, M. J. Thompson, M. Balbirnie, J. J. W. Wiltzius, H. T. McFarlane, A. Ø. Madsen, C. Riekel, and D. Eisenberg, Nature **447**, 453 (2007).

[55] S. Luca, W.-M. Yau, R. Leapman, and R. Tycko, Biochemistry **46**, 13505 (2007).

[56] A. T. Petkova, Y. Ishii, J. J. Balbach, O. N. Antzutkin, R. D. Leapman, F. Delaglio, and R. Tycko, Proc. Natl. Acad. Sci. U. S. A. **99**, 16742 (2002).

[57] Q. Cao, D. R. Boyer, M. R. Sawaya, P. Ge, and D. S. Eisenberg, Nat. Struct. Mol. Biol. **27**, 653 (2020).

[58] C. Röder, T. Kupreichyk, L. Gremer, L. U. Schäfer, K. R. Pothula, R. B. G. Ravelli, D. Willbold, W. Hoyer, and G. F. Schröder, Nat. Struct. Mol. Biol. **27**, 660 (2020).

[59] M. Assfalg, L. Ragona, K. Pagano, M. D'Onofrio, S. Zanzoni, S. Tomaselli, and H. Molinari, Biochim. Biophys. Acta, Proteins Proteomics **1864**, 102 (2016).

[60] L. E. Buchanan, E. B. Dunkelberger, H. Q. Tran, P.-N. Cheng, C.-C. Chiu, P. Cao, D. P. Raleigh, J. J. de Pablo, J. S. Nowick, and M. T. Zanni, Proc. Natl. Acad. Sci. U. S. A. **110**, 19285 (2013).

[61] L. E. Buchanan, M. Maj, E. B. Dunkelberger, P.-N. Cheng, J. S. Nowick, and M. T. Zanni, Biochemistry **57**, 6470 (2018).

[62] S.-H. Shim, R. Gupta, Y. L. Ling, D. B. Strasfeld, D. P. Raleigh, and M. T. Zanni, Proc. Natl. Acad. Sci. U. S. A. **106**, 6614 (2009).

[63] D. B. Strasfeld, Y. L. Ling, S.-H. Shim, and M. T. Zanni, J. Am. Chem. Soc. **130**, 6698 (2008).

[64] L. E. Buchanan, J. K. Carr, A. M. Fluitt, A. J. Hoganson, S. D. Moran, J. J. De Pablo, J. L. Skinner, and M. T. Zanni, Proc. Natl. Acad. Sci. U. S. A. **111**, 5796 (2014).

[65] A. Ghosh, A. K. Prasad, and L. Chuntonov, J. Phys. Chem. Lett. **10**, 2481 (2019).

[66] A. Basu, A. Vaskevich, and L. Chuntonov, J. Phys. Chem. B **125**, 895 (2021).

[67] P. M. Donaldson and P. Hamm, Angew. Chem. **125**, 662 (2013).

[68] P. Marek, A. M. Woys, K. Sutton, M. T. Zanni, and D. P. Raleigh, Org. Lett. **12**, 4848 (2010).

[69] C. T. Middleton, A. M. Woys, S. S. Mukherjee, and M. T. Zanni, Methods **52**, 12 (2010).

[70] S. D. Perrault and W. C. W. Chan, J. Am. Chem. Soc. **131**, 17042 (2009).

[71] W. Haiss, N. T. K. Thanh, J. Aveyard, and D. G. Fernig, Anal. Chem. **79**, 4215 (2007).

[72] W. B. Weeks, C. J. Tainter, and L. E. Buchanan, Biophys. J. **121**, 1549 (2022).

[73] E. B. Dunkelberger, M. Grechko, and M. T. Zanni, J. Phys. Chem. B **119**, 14065 (2015).

[74] W. B. Weeks and L. E. Buchanan, J. Phys. Chem. Lett. **13**, 9534 (2022).

[75] P. Arosio, T. P. J. Knowles, and S. Linse, Phys. Chem. Chem. Phys. **17**, 7606 (2015).

[76] C. Cabaleiro-Lago, I. Lynch, K. A. Dawson, and S. Linse, Langmuir **26**, 3453 (2010).

[77] L. Nielsen, R. Khurana, A. Coats, S. Frokjaer, J. Brange, S. Vyas, V. N. Uversky, and A. L. Fink, Biochemistry **40**, 6036 (2001).

[78] Y. S. Kim and R. M. Hochstrasser, J. Phys. Chem. B **113**, 8231 (2009).

[79] D. B. Strasfeld, Y. L. Ling, R. Gupta, D. P. Raleigh, and M. T. Zanni, J. Phys. Chem. B **113**, 15679 (2009).

[80] C. R. Baiz, B. Błasiak, J. Bredenbeck, M. Cho, J.-H. Choi, S. A. Corcelli, A. G. Dijkstra, C.-J. Feng, S. Garrett-Roe, N.-H. Ge, M. W. D. Hanson-Heine, J. D. Hirst, T. L. C. Jansen, K. Kwac, K. J. Kubarych, C. H. Londergan, H. Maekawa, M. Reppert, S. Saito, S. Roy, J. L. Skinner, G. Stock, J. E. Straub, M. C. Thielges, K. Tominaga, A. Tokmakoff, H. Torii, L. Wang, L. J. Webb, and M. T. Zanni, Chem. Rev. **120**, 7152 (2020).

[81] A. Ghosh, J. Wang, Y. S. Moroz, I. V Korendovych, M. Zanni, W. F. Degrado, F. Gai, and R. M. Hochstrasser, J. Chem. Phys. **140**, 235105 (2014).

[82] A. Ghosh, J. Qiu, W. F. DeGrado, and R. M. Hochstrasser, Proc. Natl. Acad. Sci. U. S. A. **108**, 6115 (2011).

[83] C. Fang, J. Wang, Y. S. Kim, A. K. Charnley, W. Barber-Armstrong, A. B. Smith, S. M. Decatur, and R. M. Hochstrasser, J. Phys. Chem. B **108**, 10415 (2004).

[84] E. H. G. Backus, R. Bloem, P. M. Donaldson, J. A. Ihalainen, B. Pfister, B. Paoli, A. Caflisch, and P. Hamm, J. Phys. Chem. B **114**, 3735 (2010).

[85] J. P. Lomont, J. S. Ostrander, J.-J. Ho, M. K. Petti, and M. T. Zanni, J. Phys. Chem. B **121**, 8935 (2017).

[86] M. Grechko and M. T. Zanni, J. Chem. Phys. **137**, 184202 (2012).

28 March 2024 18:01:23